Article

Towards Unlocking/Tuning the Mott Transition Temperature in Alkaline-Doped Vanadium Oxide Thermochromic Coatings and Potential Green Air-Conditioning via Room Temperature V_xO_y-V-V_xO_y Layered Coatings

B. S. Khanyile [1, 2, 3]
https://orcid.org/0000-0003-2746-7738
sfundob@gmail.com
A. Simo [1, 2]
alinesimo.aline@gmail.com

C. B. Mtshali [1]
https://orcid.org/0000-0001-5044-5575
mtshali@tlabs.ac.za
I. G. Madiba [1, 2]
https://orcid.org/0000-0002-2656-0482
madibig@unisa.ac.za
H. Swart [5]
https://orcid.org/0000-0001-5233-0130
SwartHC@ufs.ac.za
M. Duvenhage [5]
https://orcid.org/0000-0002-0631-8162
duvenhagem@ufs.ac.za
M. Henini [6]
https://orcid.org/0000-0001-9414-8492
Mohamed.Henini@nottingham.ac.uk
J. Kennedy [6]
https://orcid.org/0000-0002-9126-4997
j.kennedy@gns.cri.nz
M. Maaza [1, 2]
https://orcid.org/0000-0002-3820-7838
Maazam@unisa.ac.za

N. Numan [1, 2]
https://orcid.org/0000-0003-4026-5786
nagla@aims.ac.za
M. Nkosi [1]
https://orcid.org/0000-0002-6011-9033
m.nkosi@ilabs.nrf.ac.za
Z. M. Khumalo [1]
https://orcid.org/0000-0002-2124-0498
zakhele@tlabs.ac.za
B. Mabakachaba [1, 2, 4]
https://orcid.org/0000-0002-0977-0576
mabakachaba@gmail.com
E. Coetsee [5]
https://orcid.org/0000-0002-9214-4647
CoetseeE@ufs.ac.za
E. Lee [5]
https://orcid.org/0000-0002-4366-0469
leeE@ufs.ac.za
A. Gibaud [7]
https://orcid.org/0000-0002-7777-6427
alain.gibaud@univ-lemans.fr
M. Chaker [8]
https://orcid.org/0000-0001-9781-8842
Mohamed.Chaker@inrs.ca

1 MRD-Tandetron Accelerator & Nanosciences African Network, iThemba LABS-National Research Foundation, South Africa.
2 UNESCO-UNISA Africa Chair in Nanosciences and Nanotechnology, College of Graduate Studies, University of South Africa.
3 Maths and Physics Department, Cape Peninsula University of Technology, South Africa.
4 Department of Physics and Astronomy, University of the Western Cape, South Africa.
5 Department of Physics, University of the Free State, South Africa
6 School of Physics and Astronomy, University of Nottingham, United Kingdom.
7 Institute of Molecules and Materials, Le Mans University, France.
8 INRS-Energy and Materials, Canada

UNISA university of south africa PRESS

Nano-Horizons
https://unisapressjournals.co.za/index.php/NH
Volume 2 | 2023 | 26 pages

Nano-Horizons

https://doi.org/10.25159/3005-2602/13618
ISSN 3005-2602 (Online)

Abstract

In this contribution, we validate for the first time that the near infrared-infrared (NIR-IR) modulation of the optical transmission ($\Delta T_{TRANS} = T_{(T<TMIT)} - T_{(T>TMIT)}$) of vanadium oxide-based nanomaterials can be controlled or tuned via a genuine approach with a simultaneous drastic reduction of its Mott transition temperature T_{MIT}. More accurately, we report a significant thermochromism in multilayered $V_2O_5/V/V_2O_5$ stacks equivalent to that of pure VO_2 thin films but with a far lower transition temperature T_{MIT}. Such a multilayered $V_2O_5/V/V_2O_5$ thermochromic system exhibited a net control or tunability of the optical transmission modulation in the NIR-IR (ΔT_{TRANS}) via the nano-scaled thickness of the intermediate vanadium layer. In addition, the control of ΔT_{TRANS} is accompanied by a noteworthy diminution of the Mott transition temperature T_{MIT} from the bulk value of 68.8 °C to the range of 27.5–37.5 °C. The observed peculiar thermochromism in the multilayered $V_2O_5/V/V_2O_5$ is likely to be ascribed to a significant interfacial diffusion or an excessive interfacial stress/strain, and/or to an effective halide (Na, K, Ca) doping. This doping is driven by a significant diffusion from the borosilicate substrate surface towards the $V_2O_5/V/V_2O_5$ stacks. If the upscaling of this approach is validated, the current findings would contribute to advancing thermochromic nanomaterials and their applications in smart windows for managing solar heat and green air-conditioning technologies.

Keywords: thermochromism; solar heat management; smart windows; infrared modulation; room temperature phase transition; vanadium oxides, Mott transition tuning

1 Introduction

In accordance with current statistics, ~55% of the world's population lives in urban areas. It is projected that it would reach ~2.5 billion by 2050, with ~90% of this increase in Asia and Africa. With such an upsurge in urban population and the climate change increase of the average seasonal atmospheric temperature, air-conditioning demand in urban areas is expected to skyrocket. The global stock of air conditioners in buildings and automotives sectors is expected to rise up to ~5.6 billion by 2050 from the present exorbitant number of ~1.6 billion. The predictions of the International Energy Agency (IEA) [1] for the global energy demand in the air-conditioning sector is foreseen to triple by 2050, requiring the use of a significant additional electricity supply. This additional energy supply is expected to be equivalent to the combined current electricity capacity of the USA, the EU and Japan. Henceforth, sustainable technologies are required to minimise any related energy pressure while minimising the corresponding CO_2 footprint. Chromogenics and/or radiative cooling coatings are prospective forthcoming solutions as a sustainable corridor for green air-conditioning [2]–[10].

Amid the chromogenic diverse technologies, thermochromic materials have attracted a special interest since the observation of the reversible Mott semiconductor-metallic first

order transition in vanadium dioxide (VO_2) by Morin in 1959 [11]–[13]. Indeed, such a smart oxide exhibits a semiconductor below its phase transition temperature T_{MIT} ~ 68 °C while metallic above. Consequentially, it is optically infrared transparent and opaque below and above T_{MIT} ~ 68 °C, respectively. This reversible optical tunability in the near infrared-infrared (NIR-IR) solar spectral region allows VO_2 based coatings on glass substrate to act as smart windows (Fig. 1(a)) for solar heat management [7]–[8] if the Mott transition temperature T_{MIT} ~ 68 °C can be reduced to reach room temperature values of T_{MIT} ~ 25 °C [8].

As schematically displayed in Fig. 1(b), an ideal VO_2 based thermochromic coating should exhibit the following major characteristics: (i) a good and temperature-independent optical transmission in the visible (VIS) solar spectral range (with a priori a VIS transmission T_{VIS} > 50%), (ii) a phase transition temperature T_{MIT} close to room temperature (far below the bulk VO_2 transition of T_{MIT} ~68 °C), and (iii) a noteworthy large modulation in the NIR and IR spectral range (ΔT_{TRANS}). This modulation is defined as the difference between the optical transmissions below and above T_{MIT}; ($\Delta T_{TRANS} = T_{(T<TMIT)} - T_{(T>TMIT} > 50\%$). Although this modulation in the NIR and IR spectral range has been and still is exceedingly challenging, the lowering of the T_{MIT} and the raising of the VIS optical transmission have been successfully dealt with through an adequate doping (W, Mo . . .) or via using an additional anti-reflection treatment (TiO_2, ZrO_2, ZnO . . .), respectively [14]–[26].

In the quest for engineering optimal thermochromic VO_2 coatings with a substantial elevated modulation in the NIR-IR spectral range ($\Delta T_{TRANS} = T_{(T<TMIT)} - T_{(T>TMIT)}$), several physical and chemical methodologies were and are used for its deposition [27]–[40]. Excluding limited cases, the general use of a single and unique layer of VO_2 was and is the dominating trend in thermochromic VO_2 applications. Likewise, in its doped or un-doped form, the VO_2 based thermochromic coatings suffer regarding modulation in the infrared region (ΔT_{TRANS}). The same situation is faced even in the case of the VO_2 deposition onto various substrates; amorphous (such as glass, PET) [16]–[18], [27]–[32] or crystalline (such as quartz, silicon, mica) [27]–[32] in nature. Simply summarised, the VO_2 based thermochromic coatings suffer regarding modulation in the infrared region (ΔT_{TRANS}) in particular.

Numerous endeavours have been undertaken to comprehensively unravel the mechanism underlying the metal-to-insulator transition (MIT) in vanadium dioxide (VO_2), employing a multifaceted approach that combines both theoretical modelling and experimental investigations. Researchers have strived to gain profound insights into the intricate processes governing this phase transition, seeking to bridge the gap between theoretical predictions and empirical observations, ultimately enhancing our understanding of the unique electronic behaviour of VO_2 during the MIT [41]–[54].

In this article, we validate for the first time the possibility of the control or tunability of the NIR-IR modulation of the optical transmission (ΔT_{TRANS}). This modulation can be

controlled through an original approach with a simultaneous drastic reduction of the Mott transition temperature T_{MIT}. This original approach consists of exploiting a multilayered configuration instead of the traditional single VO_2 layer approach as illustrated in Fig. 2. In addition, it requires the use of a Magnussen V oxide such as V_2O_5 instead of the standard pure VO_2. For the validation of such an NIR-IR modulation control with a simultaneous drastic reduction of T_{MIT}, a three-layer stack consisting of $V_2O_5/V/V_2O_5$ deposited onto a glass substrate was considered. Within such a multilayered stack of $V_2O_5/V/V_2O_5$ onto a borosilicate glass substrate, the V_2O_5 layers' thickness is fixed and that of the interlayer of pure vanadium is varied followed by an additional optimal post annealing. To be precise, the thickness of the intermediate V layer was varied within the range of coalescence threshold of V thin films.

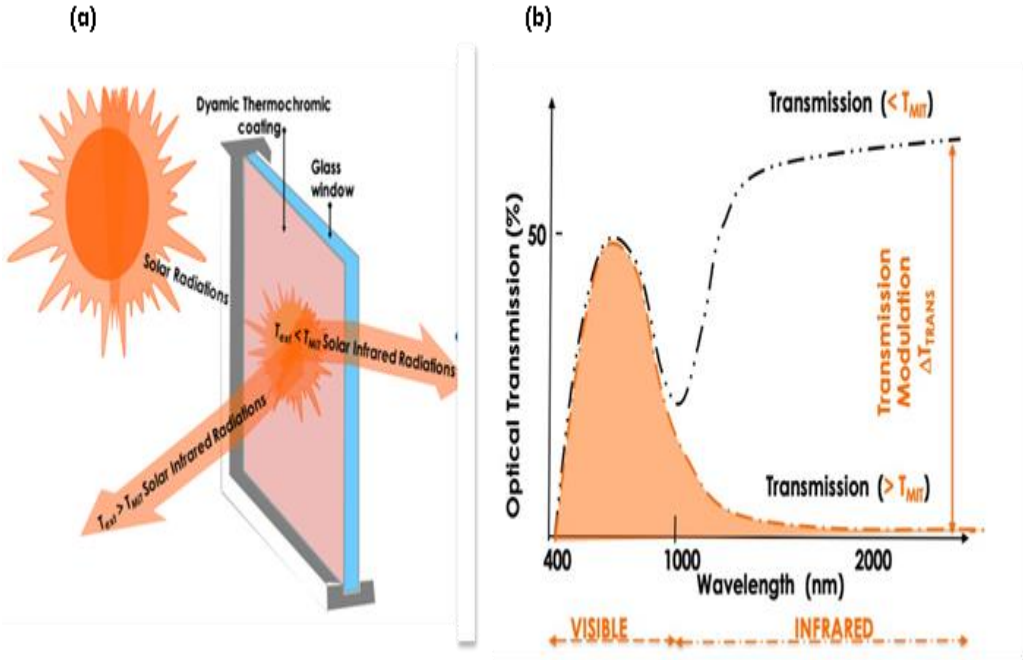

Fig. 1. Schematical representation of (a) a thermochromic based smart window, and (b) optical response of an ideal VO_x based thermochromic coating.

We emphasise that, yet original in terms of approach, this research work has been inspired by the work of Long *et al.* [27], [36], Pellegrino *et al.* [15], Miller and Wang [29], Zheng *et al.* [30], Zhou *et al.* [33], Han *et al.* [34], Zhao *et al.* [35] while fostering the previous work by Khanyile *et al.* [32].

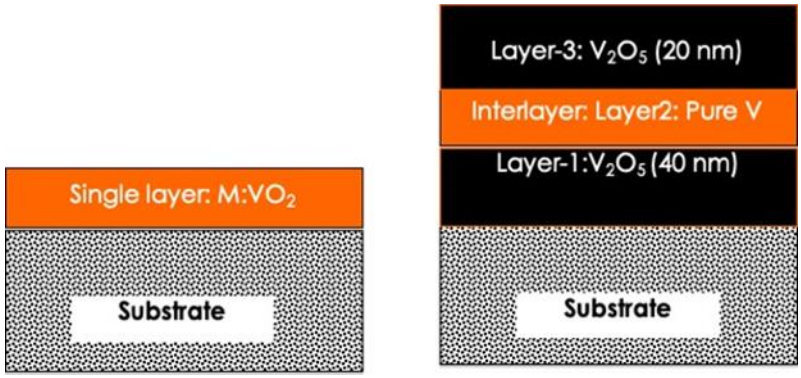

Fig. 2. The considered multilayered approach consisting of a trilayer stack of $V_2O_5/V/V_2O_5$ deposited onto a glass substrate instead of the standard configuration of single VO_2 layer approach.

In accordance with the scientific and patented published literature, and as it was highlighted previously, other multilayered nanostructures were proposed but none allowed a significant control of the NIR-IR modulation with a colossal decrease of the T_{MIT} simultaneously without the standard W or Mo doping. Table I summarises such multilayered nanostructures.

TABLE I
MAJOR PUBLISHED VO_2 BASED MULTILAYERED COATINGS

Configuration of the multilayered system	**Synthesis technique**	**Transition temperature T_{MIT} (°C)**	**References**
V_2O_3/VO_2	Reactive magnetron sputtering	72.0	Long *et al.* [27]
VO_2/TiO_2	Pulsed laser deposition	63.5	Pellegrino *et al.* [15]
$ITO/VO_2/TiO_2$	Reactive magnetron sputtering	52.0	Wang & Miller [29]
$TiO_2/VO_2/TiO_2$	Medium frequency reactive magnetron sputtering	61.5	Zheng *et al.* [30]
SiO_2/VO_2	Spin coating	61.0	Wang *et al.* [31]
V_2O_3/V (7 nm)$/V_2O_3$	Electron beam evaporation with a non-optimised annealing	27.9	Khanyile *et al.* [32]
V_2O_3/V(12 nm)$/V_2O_3$	Electron beam evaporation with a non-optimised annealing	36.9	Khanyile *et al.* [32]
$VO_2/Au/VO_2$	Electron beam evaporation	66.9	Zhou *et al.* [33]

Configuration of the multilayered system	Synthesis technique	Transition temperature T_{MIT} (°C)	References
$V_2O_5/V/V_2O_5$	Electron beam evaporation	high-temp. coefficient of resistance	Han *et al.* [34]
SiO_2-$TiO_2/VO_2/TiO_2$	Spin coating	36.9	Zhao *et al.* [35]
$WO_3/VO_2/WO_3$	Reactive magnetron sputtering	54.5	Long *et al.* [36]
V_2O_5/V(7 nm)/V_2O_5	Electron beam evaporation with an optimised annealing	27.5	Current work
V_2O_5/V(12 nm)/V_2O_5	Electron beam evaporation with an optimised annealing	37.5	Current work

In the following experimental section, we investigate three $V_2O_5/V/V_2O_5$ stacks to validate the effectiveness of the proposed approach. From an engineering viewpoint, it would be suitable to scale up such a validated thermochromic procedure on large surfaces to benefit the air-conditioning sector.

2 Materials and Methods

2.1 Sample Preparation

All chemicals and substrates used in these experiments are of high chemical grade (from Sigma-Aldrich and/or Alfa Aesar). Following a sequential procedure, multilayered films of $V_2O_5/V/V_2O_5$ were deposited by e-beam evaporation using V_2O_5 powder and V metal material targets and borosilicate glass substrates (10×10 mm^2). The substrates were cleaned in an ultrasonic bath with methanol and deionised water for ~20 min before deposition. All substrates were dried with pressurised 100% pure N_2 gas before being loaded into the deposition chamber, which was already loaded with highly pure vanadium (V) and vanadium pentoxide (V_2O_5) targets in separate crucibles. The multilayered stacks were deposited at an initial chamber vacuum pressure of ~10^{-6} mbar and an evaporation rate of ~0.24 nm/s. The V_2O_5 and pure V layers' thicknesses were monitored with a standard crystal monitor. The thickness of the first layer (bottom layer) of V_2O_5 was fixed to ~40 nm, while the thickness of the intermediate layer (V layer) was varied within a defined range of 3–12 nm at specific values of 3, 7 and 12 nm. The thickness of the third layer (top layer) of (V_2O_5) was fixed at 20 nm. These thicknesses were chosen based on a preliminary set of computations, which suggested that the film be chosen in such a way that sufficient diffusion of oxygen into that interlayer would take place besides an additional interfacial stress/strain; with both layers allowing O atoms to diffuse into the V intermediate layer. All prepared samples were annealed for 120 min in a vacuum of ~10^{-6} mbar at the temperature of 500 °C.

2.2 Sample Characterisation

The surface morphology of the samples was investigated using atomic force microscopy (AFM) in non-contact mode complemented by in-depth/volume morphology studies using a field emission scanning electron microscopy (FE-SEM, Jeol JSM-7800F). The crystal structure of the various samples was examined with a Bruker AXS D8 advanced X-ray diffractometer, which was outfitted with a copper X-ray tube (λ = 0.15406 nm) and operated at 40 kV and 40 mA with data collection in the Θ-2Θ configuration within the angular range of 15–60 deg. (in steps of 0.01 deg.). For the elemental analysis and depth profiling, auger electron spectroscopy (AES) and time-of-flight secondary ion mass spectrometry (ToF-SIMS) were used. The optical measurements within the spectral range of 250-2 500 nm were carried out in transmittance mode (normal incidence) with a Cary 5000 UV-VIS-NIR spectrometer equipped with a controllable heating stage with a heating/cooling rate of 5 °C/min within the temperature range of 20–90 °C.

3 Results and Discussion

3.1 Morphological Investigations: Atomic Force Microscopy and Field Emission Scanning Electron Microscopy Studies

Fig. 3(a) displays the AFM of the various samples. The surfaces are relatively rough suggesting, a priori, the crystalline nature of the multilayered stack samples or at least the top surface of layer three of V_2O_5. Table II summarises the corresponding values of the average roughness (R_a), the root mean square (R_σ), the average height (H) as well as the average crystallites size (Ø). Accordingly, the intermediate V layer is thicker and the various parameters ($<R_a>$, $<R_\sigma>$, <H> and <Ø>) are higher. Yet limited to three values of the intermediate V layer's thickness, it can be safely concluded that the effect of the intermediate V layer's thickness is of a prime effectiveness as sustained by the variations summarised in Table II and Fig. 3(b).

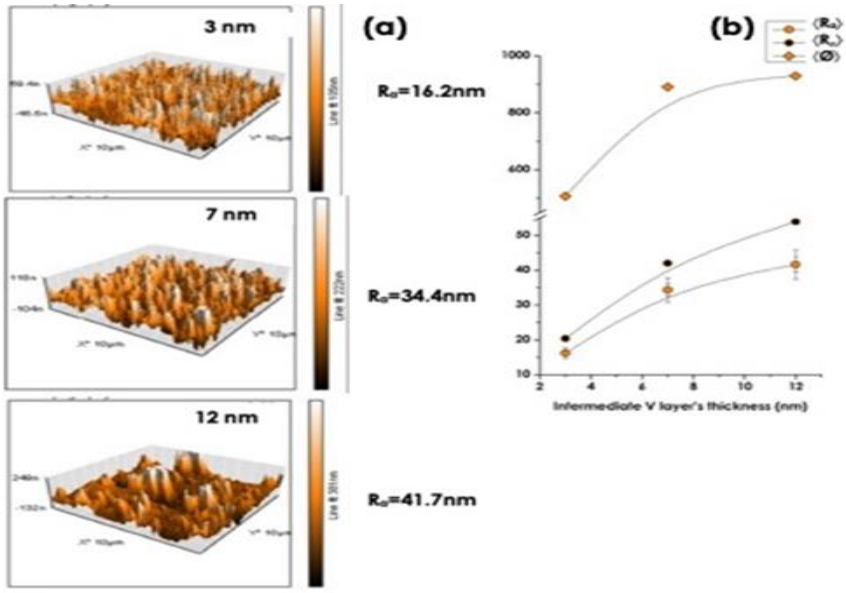

Fig. 3. (a) AFM surface morphology scans of the various multilayered stacks of $V_2O_5/V/V_2O_5$ deposited onto a borosilicate glass substrate, (b) Variation of the average roughness (Ra), the root mean square (Rσ), as well as the average crystallites size (Ø) versus the intermediate vanadium layer's thickness.

TABLE II

CORRESPONDING VALUES OF THE AVERAGE ROUGHNESS (R_a), THE ROOT MEAN SQUARE (R_σ), THE AVERAGE HEIGHT (H) AND THE AVERAGE CRYSTALLITES SIZE (Ø)

Sample identification	**Intermediate V layer thickness (nm)**	**Average roughness (Ra) (nm)**	**Root mean square roughness (R_σ) (nm)**	**Average height H (H) (nm)**	**Average grain size (Ø) (nm)**
V2O5/3nmV/V2O5	3	16.21	20.39	1.04	507.82
V2O5/7nmV/V2O5	7	34.37	42.04	2.36	890.62
V2O5/12nmV/V2O5	12	41.65	53.93	2.47	929.76

Fig. 4 displays the FE-SEM edge cross section of the various multilayered stack samples. It is not possible to distinguish the various layers of the stacks $V_2O_5/V/V_2O_5$ deposited onto the borosilicate glass substrate in each of the samples. Indeed, excluding the clear net interface with the substrate, there are no sharp interfaces between the bottom layer one (V_2O_5), the intermediate V layer and the top layer three (V_2O_5). This is a signature of a noteworthy interfacial diffusion within both interfaces of the intermediate layer of V and top or bottom surrounding layers of V_2O_5. This seems to be supported by the observed various nanocrystals distributed in a homogeneous way

within the transversal direction of the stack throughout the two interfaces as shown in Fig. 4. If one considers the O and V atomic/ionic radii, it could be safely concluded that oxygen is likely to diffuse from the O rich regions, ie from layers one and three of V_2O_5 towards the O poor region (the pure V intermediate layer). Last but not least, one can observe several cracks within the substrate of sample three, ie the 12 nm V intermediate layer thickness. These cracks seem to be initiated from layer one substrate interface and propagating towards the inner section of the substrate. These cracks are likely to originate from a significant stress or strain relaxation at the interface layer one/substrate at least. As a preliminary conclusion of this section, one could cautiously emphasise the elevated interfacial diffusion within the interfaces (top and bottom) surrounding the intermediate layer of pure vanadium. Such a significant interfacial diffusion would not only affect the chemical composition profile of the multilayered stack but also the strain or stress distribution.

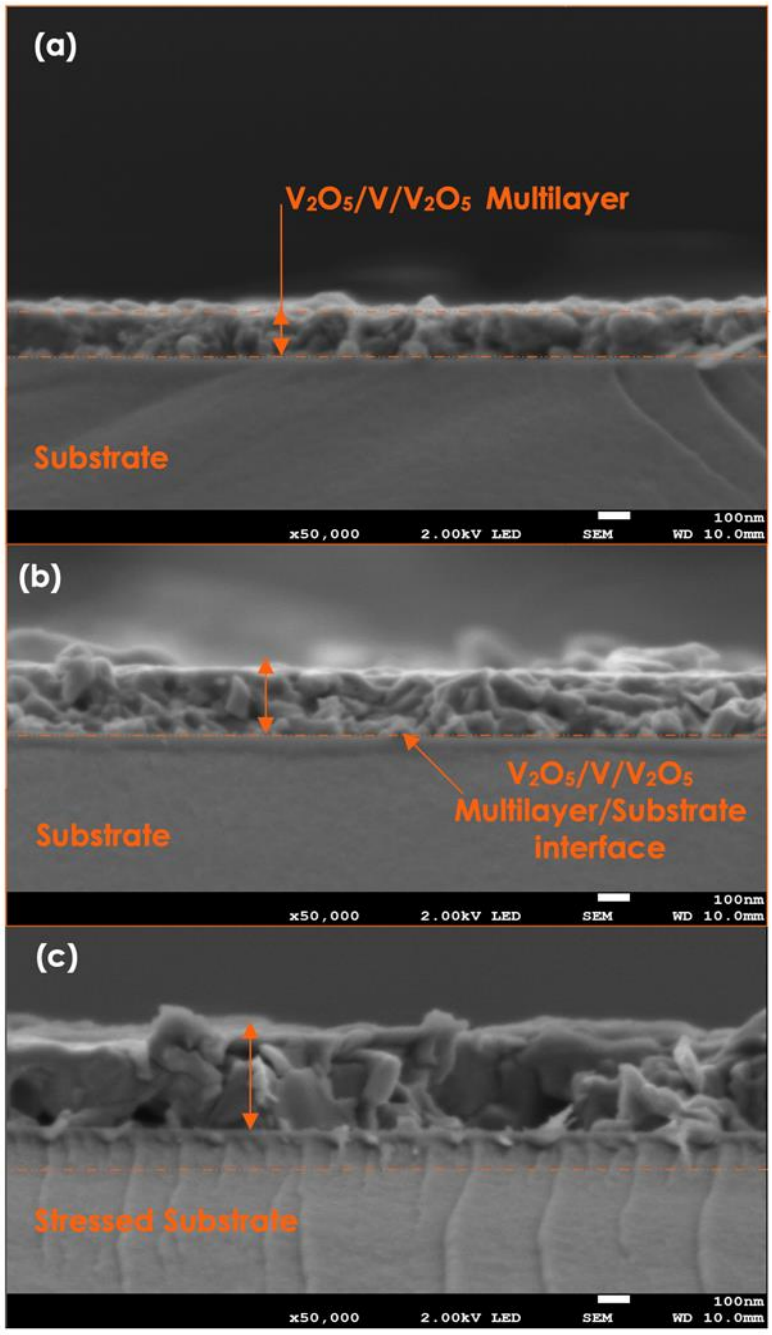

Fig. 4. FE-SEM edge cross section of the of the various multilayered stacks of $V_2O_5/V/V_2O_5$ deposited onto the borosilicate glass substrate for various intermediate vanadium layer's thickness; (a) 3 nm, (b) 7 nm and (c) 12 nm.

3.2 Elemental Analysis: Auger Spectroscopy Depth Profiling Studies

Fig. 5 shows the corresponding depth variation of the O/V ratio deduced from the Auger spectroscopy depth profiling analysis. One can clearly notice the presence of oxygen throughout the transversal direction of the three stacks. This is in support of the significant interfacial diffusion mentioned previously, especially the O diffusion from the surrounding V_2O_5 towards the intermediate V layer. Likewise, and accordingly and within the bar error of 5%, the average value of the O/V ratio seems increasing quasi linearly for sample one ($V_{Intermediate\text{-}layer}$ = 3 nm) while fluctuating between 1.5 and 2 for sample two ($V_{Intermediate\text{-}layer}$ = 7 nm) and sample three ($V_{Intermediate\text{-}layer}$ = 12 nm). Henceforth, it can safely be concluded that in the two thicker stacks, the dominating phase is within the V_2O_3 and VO_2 families from a stoichiometric viewpoint and/or phases under significant strain or stress (if one considers the observed cracks relaxation in the FE-SEM images of Fig. 4).

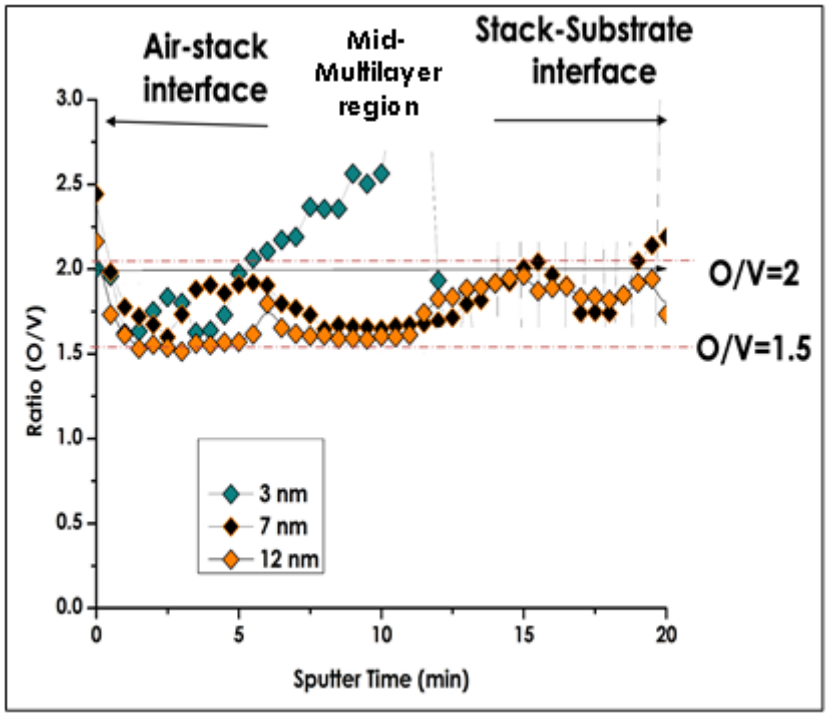

Fig. 5. In-depth profile O/V ratio variation derived from Auger spectrometry elemental depth profiling of oxygen (O) and vanadium (V) of the various multilayered stacks of V_2O_5/V/V_2O_5 deposited onto the borosilicate glass substrate for various intermediate vanadium layer's thickness; 3 nm, 7 nm, and 12 nm.

3.3 Elemental Analysis: Studies of Secondary Ion Mass Spectrometry Depth Profiling

Fig. 6 displays the elemental depth profiling of several ions proper to the stack (V^+, VO^+) and those from the borosilicate substrate (Na^+, Ca^+ and K^+) in view of investigating various interfacial diffusion phenomena. These explicit ions were targeted in view of the chemical composition of the borosilicate glass substrate (consisting of SiO_2:72.5%, Na_2O:13.7%, CaO:9.1%, KO:12%, MgO:4.2% . . .) [54]. Once again, the distribution profiles of V^+, VO^+ are alike throughout the multilayered stack samples and the stack–substrate interface. This matching depth distribution of V^+ and VO^+ is in strict support of the O diffusion observed in the previous Auger profiles.

The Si profiles exhibit a heavy-side type variation for each of the samples with nearly zero counts within the stack in support of a very weak or no diffusion of Si originating from the substrate. Contrasting with such a Si limited interfacial diffusion is the alkaline ions, namely, Na^+, Ca^+ and K^+. All of them display a long-range diffusion from the borosilicate glass throughout the stacks with Na^+ followed by K^+ and Ca^+ up to the air-stacks interface. Such a prominent extended diffusion is likely due to a small ionic radius ($Ø_{Na+} \approx 0.102$ nm, $Ø_{K+} \approx 0.138$ nm, $Ø_{Ca+} \approx 0.118$ nm) and low activation energy of the concerned alkaline and subsequently their elevated diffusion coefficient ($D_{Na+} \approx 1.330 \times 10^{-9}$ m^2/s, $D_{K+} \approx 1.960 \times 10^{-9}$ m^2/s, $D_{Ca+} \approx 0.793 \times 10^{-9}$ m^2/s) by contrast to Mg, Si and V. However, there is a clear difference between the depth distributions of Na^+, Ca^+ and K^+. Relatively to Na^+, Ca^+ profiles, the profile of K^+ is singular. While its depth distribution is inhomogeneous for stack one (intermediate $V_{layer} = 3$ nm), it is very low and nearly constant throughout the $V_2O_5/V/V_2O_5$ stacks two and three (intermediate $V_{layer} = 7$ and 12 nm). In addition, the K^+ profiles display a net localised peak at the interface substrate stacks two and three. While such an accumulation at the substrate multilayered stacks interface is not understood, the constant diffusion within the multilayered stacks up to the air multilayered stacks interface would likely affect the thermochromic properties, if any.

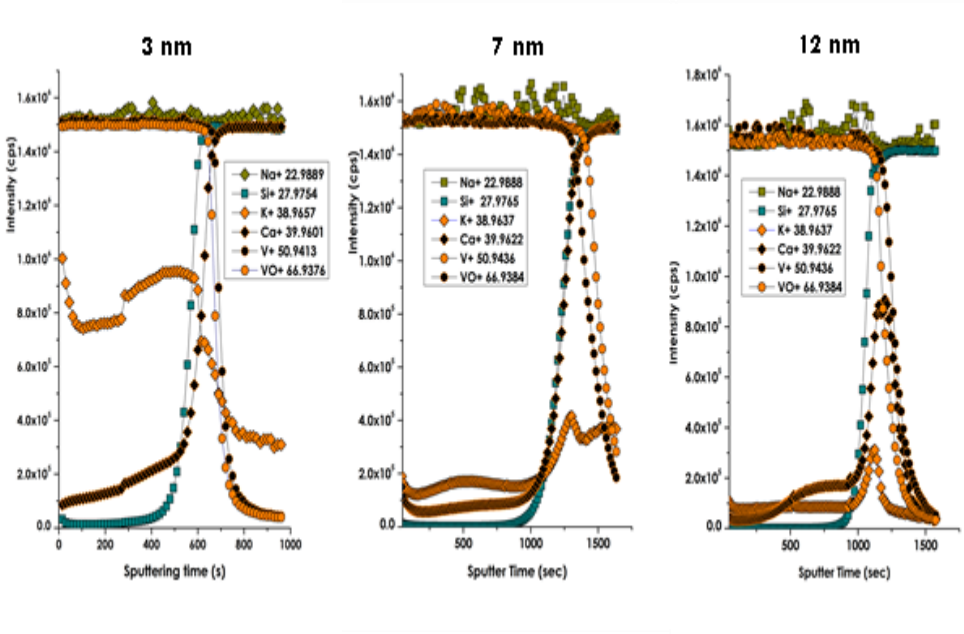

Fig. 6. In-depth profile O/V ratio variation derived from SIMS elemental depth profiling of various halides (Na, K, Ca), Silicon Si^{+}, vanadium (V^{+}) and VO^{+} of the various multilayered stacks of $V_2O_5/V/V_2O_5$ deposited onto the borosilicate glass substrate for various intermediate vanadium layer's thickness; 3 nm, 7 nm, and 12 nm.

3.4 Crystallographic Properties: Texture and Crystallites Orientations

Fig. 7 reports the room temperature X-ray diffraction pattern of the three multilayered stacks of $V_2O_5/V/V_2O_5$ onto the borosilicate glass substrate within the Θ-2 Θ diffraction configuration. The pattern was zoomed onto the angular region of 25–31 deg. Such an angular limitation is due to the fact there were no diffraction signatures below 25 deg. and above 31 deg. On the other hand, one can clearly distinguish the (011) main Bragg diffraction peak of the monoclinic VO_2 thermochromic active phase which for the bulk or non-strained VO_2 thin films generally is centred on $2\Theta \sim 27.85$ deg. Nevertheless, those observed on the investigated samples are displaced toward higher values by at least ~1 deg. (samples two and three). Such an angular shift can only be ascribed to a significant compressive strain or stress on the various (011) reticular planes. The relative compression on such a set of reticular atomic planes is of the order of $\Delta d_{011}/d_{011} \sim \Delta\Theta_{011}/\tan\Theta_{011} \sim 3.5\%$ for samples one and two corresponding to the intermediate V layer of 7 and 12 nm. On the other hand, the one corresponding to the thinnest intermediate V layer, ie 3 nm, seems to be under a far higher strain or stress in view of the larger angular shift of almost ~ 1.73 deg.

It is to be mentioned that this sample's XRD profile exhibits a rich diffraction pattern with three consecutive potential low intensity Bragg peaks centred approximately on the vicinity of 27.07, 28.29 and 29.90 deg. This set of low intensity peaks may correspond to a substructure within the first sample ($V_{Intermediate\text{-}layer}$ = 3 nm), if any. To shed light correctly on the nature of such a rich diffraction pattern, it would require, a priori, synchrotron type investigations, grazing incidence x-rays diffraction studies [37]–[39] in particular. As a preliminary conclusion of this crystallographic investigation study, it is safe to deduce that there is significant strain or stress on the nanocrystals and their atomic reticular plans especially those of (011) orientation.

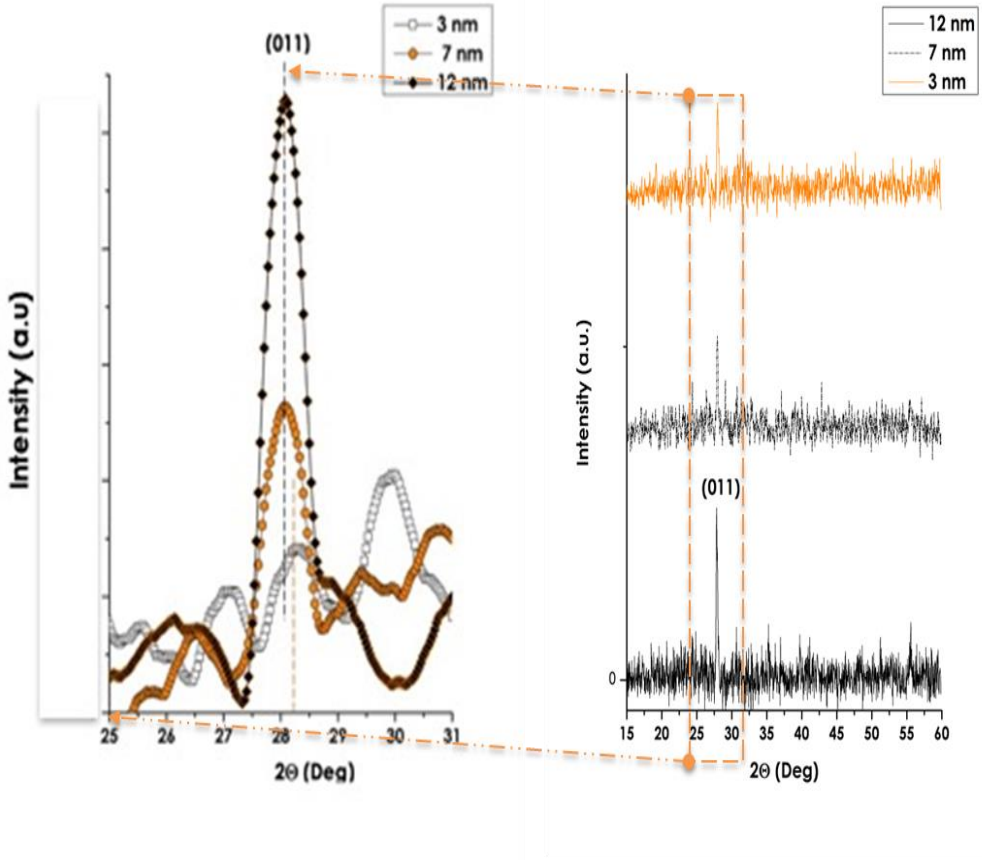

Fig. 7. (a) The room temperature X-ray diffraction pattern of the various multilayered stacks of $V_2O_5/V/V_2O_5$ deposited onto the borosilicate glass substrate for various intermediate vanadium layer's thickness; 3nm, 7 nm and 12 nm., in full angular range of 15–60 deg.

3.5 Optical Properties: NIR-IR Modulation Tunability and Control

Fig. 8(a) shows the central decisive results of this study. It displays the experimental optical transmission profiles of the three multilayered stacks of $V_2O_5/V/V_2O_5$ onto the borosilicate substrate within the spectral range of 250–2 500 nm below and above the transition temperature T_{MIT} ~ 68 °C, at 25 °C and 70 °C in particular. Herein, they are labelled as cooling and heating, respectively. In Fig. 8(a), all of the three multilayered stacks exhibit a thermochromic signature with a crystal dependence on the intermediate vanadium layer's thickness regarding T_{VIS} and the NIR-IR modulation ΔT_{TRANS}. This modulation is about 1.47%, 42.01% and 32.10% for the V_2O_5/3 nm V/V_2O_5, V_2O_5/7 nm V/V_2O_5, and V_2O_5/12 nm V/V_2O_5 samples, respectively. Accordingly, and within this multilayered configuration of the $V_2O_5/V/V_2O_5$/ glass substrate, it is therefore safe to conclude that the targeted control of the modulation of ΔT_{TRANS} versus the intermediate V layer's thickness is validated.

Fig. 8(b) and (c) show the VIS (250–1 000 nm) and NIR-IR (1 000–2 500 nm) spectral ranges. In addition to the modulation in the NIR and IR, the transmission in the VIS spectral range is also affected, although slightly. The corresponding maximum of the optical transmission $<T_{VIS}>$ is about 60.53%, 22.62% and 46.48% for the V_2O_5/3 nm V/V_2O_5, V_2O_5/7 nm V/V_2O_5, V_2O_5/12 nm V/V_2O_5 samples, respectively. By contrast to single VO_2 thermochromic coatings, the wavelength corresponding to the maximum of transmission in the VIS spectral range is varying with the intermediate V layer's thickness too. The spectral position of such a maximum of transmission λ^{Max}_{VIS} is centred approximately on 528.7, 682.6 and 665.1 nm for the V_2O_5/3 nm V/V_2O_5, V_2O_5/7 nm V/V_2O_5, V_2O_5/12 nm V/V_2O_5 samples, respectively.

Fig. 8(d) displays the evolution of the average optical transmission in the VIS; $<T_{VIS}>$ and the optical transmission modulation in the NIR-IR ΔT_{TRANS} ($\Delta T_{TRANS} = T_{(T<TMIT)} - T_{(T>TMIT)}$). The figure seems indicating that $<T_{VIS}>$ and ΔT_{TRANS} variations versus the thickness of the intermediate V layer are in opposition of phase within the considered configuration of $V_2O_5/V/V_2O_5$/ onto the borosilicate glass substrate. This seems indicating that there is still room for optimisation of ΔT_{TRANS} with a sort of trade-off between $<T_{VIS}>$ and ΔT_{TRANS} (as shown in the shaded region of Fig. 8(d)). See also Table III.

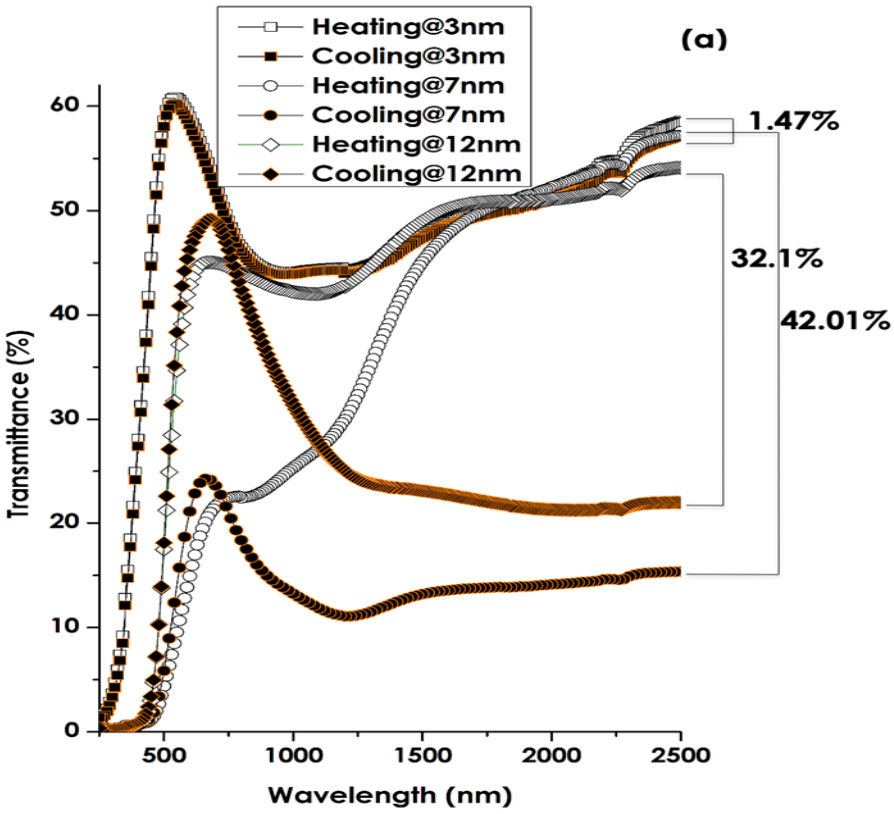

Fig. 8. (a) The experimental optical transmission profiles of the various multilayered stacks of $V_2O_5/V/V_2O_5$ deposited onto the borosilicate glass substrate for the intermediate vanadium layer's thickness; 3nm, 7 nm and 12 nm.

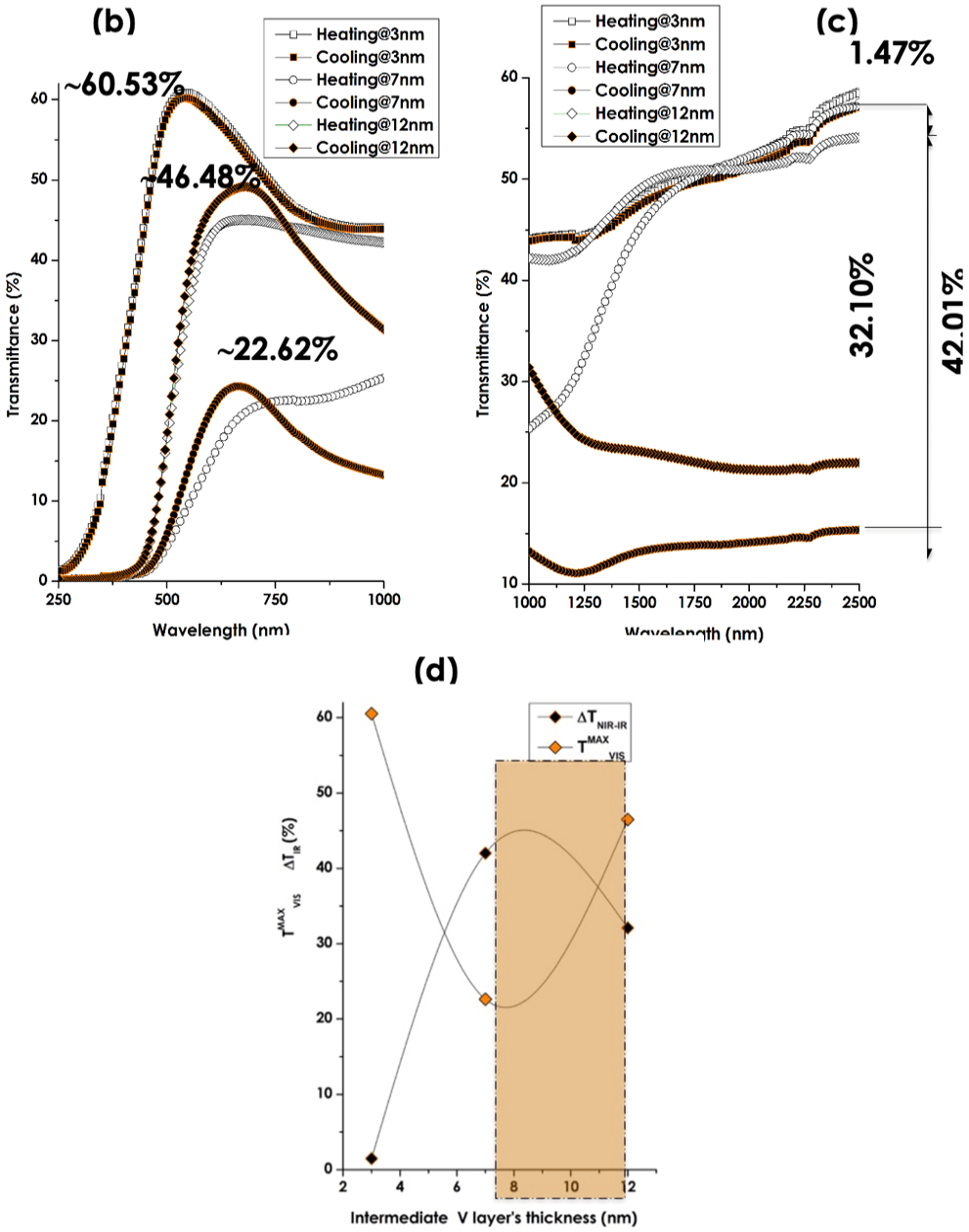

Fig. 8. (b) and (c) The VIS spectral region (250–1 000 nm) and the NIR-IR spectral region (1 000–2 500 nm) respectively, (d) The evolution of the average optical transmission in the VIS; T_{VIS} and the optical transmission modulation in the NIR-IR, ($\Delta T_{TRANS} = T(_{T>TMIT}) - T(_{T<TMIT})$ versus the intermediate vanadium layer's thickness.

TABLE III

VARIATION OF THE MAJOR OPTICAL PARAMETERS VERSUS THE INTERMEDIATE V LAYER'S THICKNESS; MAXIMUM VIS TRANSMISSION WAVELENGTH $<\lambda_{VIS}>$, MAXIMUM VIS TRANSMISSION WAVELENGTH $<T_{VIS}>$, AND THE NIR-IR MODULATION ΔT_{TRANS} ($\Delta T_{TRANS} = T_{(T<TMIT)} - T_{(T>TMIT)}$)

Sample Identification	Intermediate V Layer Thickness (nm)	Maximum VIS Transmission Wavelength $\langle\lambda_{VIS}\rangle$, (nm)	Average VIS Transmission $\langle T_{VIS}\rangle$, (%)	Maximum Transmission $T_{(T\langle TMIT)}$, (%)	Minimum Transmission $T_{(T\rangle TMIT)}$, (%)	Transmission Modulation (ΔT_{TRANS}), (%)
V_2O_5/3nmV/V_2O_5	3	528.7	60.53	58.58	57.11	1.47
V_2O_5/7nmV/V_2O_5	7	682.6	46.48	54.02	21.92	32.1
V_2O_5/12nmV/V_2O_5	12	665.1	22.62	57.33	15.32	42.01

In addition to the morphological and interfacial diffusion aspects, the major findings so far identified were quantified with regard to the visible optical transmission T_{VIS} and specifically the NIR-IR optical modulation ΔT_{TRANS}.

Finally, it is necessary to shed light on the effective transition temperature of the investigated multilayered stacks and its evolution versus the intermediate vanadium layer's thickness, if any. This temperature should be stress or strain related in view of the non-negligible large lattice mismatch between the V_2O_5 and V layers and the alkaline elements diffusion. Both the crystalline lattice mismatch and the diffused alkaline elements would likely induce a noteworthy stress or strain. This stress or strain would likely induce a reduction of the transition temperature of the stack as was reported in the literature by various authors [40]–[53].

The hysteresis measurements were subsequently carried out on the various samples as shown in Fig. 9(a). Fig. 9(a) displays the common hysteresis of the transmission versus the temperature for a fixed wavelength (2 500 nm) for the multilayered stack corresponding to the intermediate vanadium layer's thickness of 7 and 12 nm. The hysteresis for the 3 nm V was inconsequential and therefore omitted. The width of the hysteresis for both the 7 and 12 nm V layer's thickness are almost similar in the order of $\delta T \sim 7$ °C. This value is relatively smaller than the generally reported hysteresis of single VO_2 thin films which is in the order of $\delta T \sim 10$ °C. The low value of the hysteresis. ($\delta T \sim 7$ °C) might be due to the initial large density of nucleating defects during the films growth as observed and concluded by Zhang *et al.* [51].

To estimate the corresponding transition temperatures, the standard derivative approach is used. Fig. 9(b) and (c) display the corresponding derivative hysteresis profiles. The average of the corresponding minima is 27.5 °C and 37.5 °C for the V_2O_5/V/V_2O_5 multilayered stacks with the intermediate vanadium layer's thickness of 7 and 12 nm, respectively. This substantial lowering of the T_{MIT}, which is the second prominent

finding of this study, is likely to be ascribed to the above-mentioned interfacial diffusion and/or stress or strain as well as the alkaline diffusing elements. This parameter was found to be pivotal in significantly affecting the crystallographic properties but mostly the corresponding electronic response in view of the electronic orbitals‘ configuration [48]–[51].

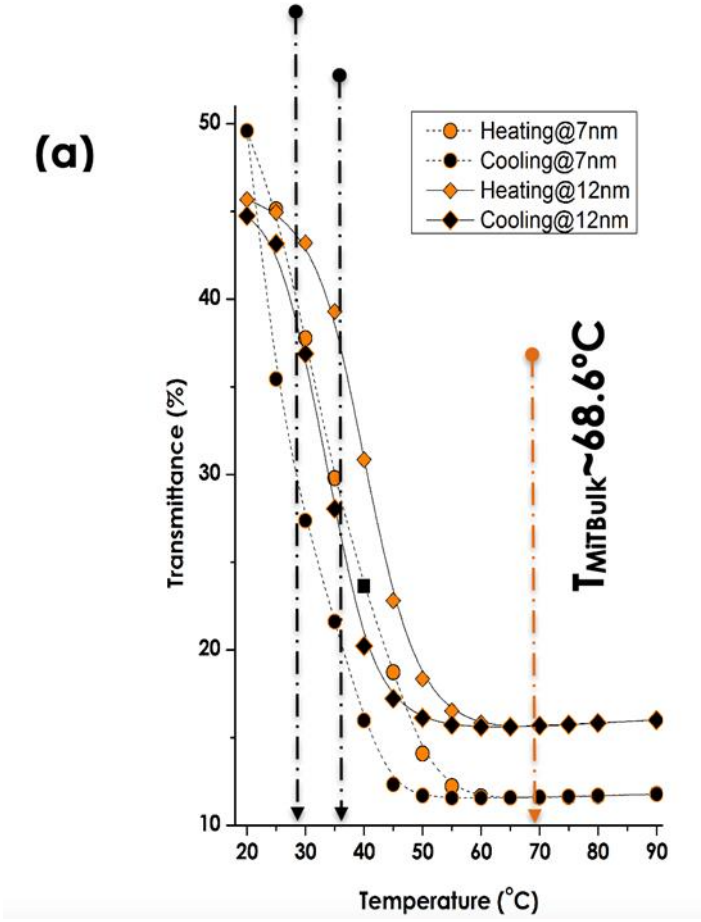

Fig. 9. (a) The standard hysteresis of the transmission versus the temperature for a fixed wavelength (2 500 nm) for the multilayered stack corresponding to the intermediate vanadium layer‘s thickness of 7 and 12 nm.

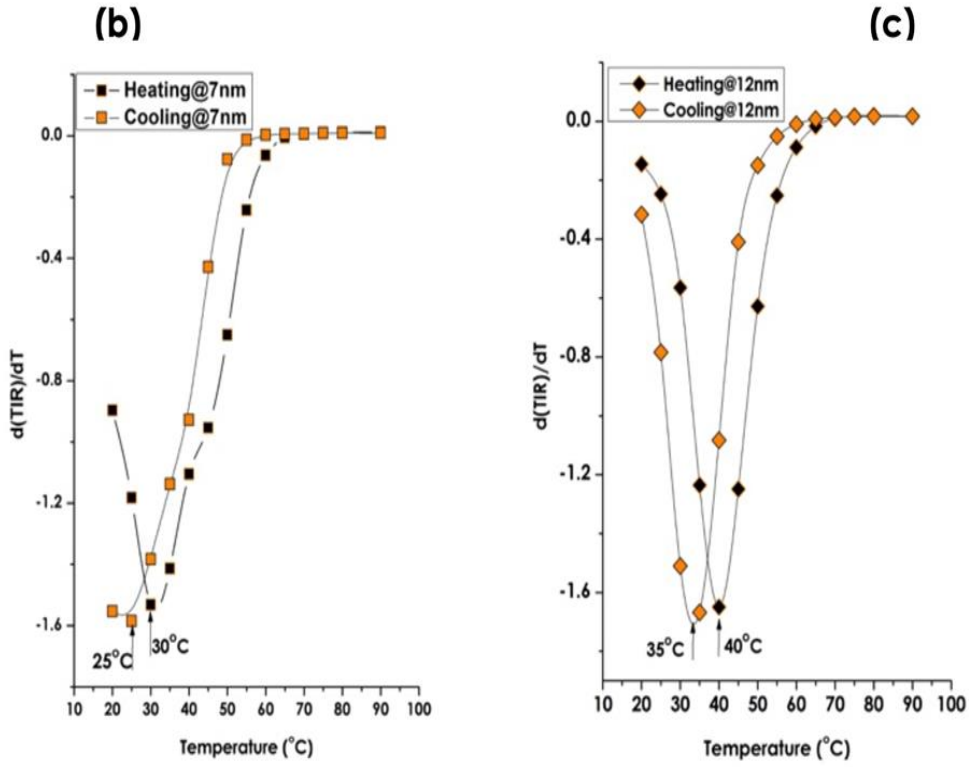

Fig. 9. (b) and (c) Corresponding derivative hysteresis profiles of $V_2O_5/V/V_2O_5$ deposited onto the borosilicate glass substrate with the intermediate vanadium layer‘s thickness of 7 and 12 nm, respectively.

As a preliminary conclusion, one might consider with provision that the investigated $V_2O_5/V/V_2O_5$ stacks (with 7 and 12 nm V layer’s thickness) onto the borosilicate glass substrate behave as a hypothetic thermochromic VxOy phase. This phase exhibits a thickness dependent NIR-IR ΔT_{TRANS} with a lower phase transition temperature of T_{MIT} = 27.5 or 37.5 °C while under a stern interfacial stress or strain and in the presence of dopant alkaline diffusing elements (Na^+, K^+, Ca^+) originating from the borosilicate glass substrate.

4 Conclusion

In this article, we validated the thermochromic properties of a novel configuration consisting of $V_2O_5/V/V_2O_5$ stacks deposited onto borosilicate glass substrates by electron beam deposition. While the thickness of the V_2O_5 top and bottom layers was fixed, that of the intermediate V layer was varied within the range of 3–12 nm, ie within the coalescence threshold of vanadium. Such a system exhibited a clear thermochromic behaviour similar at a certain extent to that of VO_2 but with a lower T_{MIT} and controllable

thermochromic optical modulation in the NIR-IR; ($\Delta T_{TRANS} = T_{(T<TMIT)} - T_{(T>TMIT}$). This modulation was controllable via the intermediate V layer's thickness. A significantly large stress or strain on the $V_2O_5/V/V_2O_5$ stacks was observed. In addition, a paramount diffusion of alkaline elements from the substrate into the full stack is observed. The combination of such a strain or stress and alkaline elements diffusion has induced a significant low-phase transition temperature T_{MIT} within the range of 27.5 to 37.5 °C. It could be concluded that the $V_2O_5/V/V_2O_5$ multilayered stacks could be considered the equivalent of a hypothetical under stress or strain alkaline-doped V_xO_y phase with a phase transition close to room temperature and a tunable NIR-IR optical transmission modulation.

5 Acknowledgements

We are grateful to the following supporting institutions:

- the University of South Africa;
- iThemba LABS;
- the National Research Foundation of South Africa;
- the African Laser Centre;
- the international Organization of Women in Science;
- the Abdus Salam International Centre for Theoretical Physics;
- the Royal Society of London;
- the German Academic Exchange Service;
- the United Nations Education, Scientific and Cultural Organization;
- the French Foreign Ministry;
- the French ADESFA programme; and
- the Centre for High Performance Computation.

6 Availability of Data and Materials

The data sets used and/or analysed during the current study are available from the corresponding authors on request.

7 References

[1] International Energy Agency, "Building envelopes," n.d. [Online]. Available: https://www.iea.org/energy-system/buildings/building-envelopes.

[2] D. M. Kammen and D. A. Sunter, “City-integrated renewable energy for urban sustainability,” *Sci*, vol. 352, pp. 922–928, 2016, doi: 10.1126/science.aad9302.

[3] J. Rogelj *et al.*, “Energy system transformations for limiting end-of-century warming to below 1.5 °C,” *Nature Clim. Change*, vol. 5, pp. 519–527, 2015, doi: 10.1038/nclimate2572.

[4] C. Sui *et al.*, “Dynamic electrochromism for all-season radiative thermoregulation,” *Nat. Sustain.*, vol. 6, pp. 428–437, 2023, doi: 10.1038/s41893-022-01023-2.

[5] K. Tang *et al.*, “Temperature-adaptive radiative coating for all-season household thermal regulation,” *Sci.*, vol. 374, pp. 1504–1509, 2021, doi: 10.1126/science.abf7136.

[6] N. N. Shi *et al.*, “Keeping cool: Enhanced optical reflection and radiative heat dissipation in Saharan silver ants,” *Sci*, vol. 349, pp. 298–301, 2015, doi: 10.1126/science.aab3564.

[7] C. Jorgensen, “Electrochromic and thermochromic materials for solar energy applications with emphasis on niobium and vanadium oxides,” Lawrence Berkeley, Berkeley, CA, USA, Laboratory Report (LBL-18299), August 1984.

[8] C. G. Granqvist, *Handbook of Inorganic Chromogenic Materials*, Amsterdam: Elsevier, 1995.

[9] X. Li *et al.*, “Integration of daytime radiative cooling and solar heating for year-round energy saving in buildings,” *Nat. Commun.*, vol. 11, p. 6101, 2020, doi: 10.1038/s41467-020-19790-x.

[10] B. P. Jelle, S. E. Kalnæs and T. Gao, “Low-emissivity materials for building applications: A state-of-the-art review and future research perspectives,” *Energy Build.*, vol. 96, pp. 329–356, 2015, doi: 10.1016/j.enbuild.2015.03.024.

[11] F. J. Morin, “Oxides which show a metal-to-insulator transition at the neel temperature,” *Phys. Rev. Lett. 3*, p. 34, 1959, doi: 10.1103/PhysRevLett.3.34.

[12] D. Adler, “Mechanisms for metal-nonmetal transitions in transition-metal oxides and sulfides,” *Rev. Mod. Phys.*, vol. 40, p. 714, 1968, doi: 10.1103/RevModPhys.40.714.

[13] S. Wang *et al.*, “Scalable thermochromic smart windows with passive radiative cooling regulation,” *Sci.*, vol. 374, pp. 1501–1504, 2021, doi: 10.1126/science.abg0291.

[14] S. Chen *et al.*, “The visible transmittance and solar modulation ability of VO_2 flexible foils simultaneously improved by Ti doping: An optimization and first principle study,” *Phys. Chem. Chem. Phys.*, vol. 15, p. 17537, 2013, doi: 10.1039/c3cp52009a.

[15] L. Pellegrino *et al.*, “Multistate memory devices based on free-standing VO_2/TiO_2 microstructures driven by joule self-heating,” *Adv. Mater.*, vol. 24, no. 21, pp. 2929–2934, 2012, doi: 10.1002/adma.201104669.

[16] M. Jiang *et al.*, "Improved luminous transmittance and diminished yellow color in VO_2 energy efficient smart thin films by Zn doping," *Ceram. Int.*, vol. 40, no. 4, pp. 6331–6334, 2013, doi: 10.1016/j.ceramint.2013.10.083.

[17] Y. Wu *et al.*, "Decoupling the lattice distortion and charge doping effects on the phase transition behavior of VO_2 by titanium (Ti^{4+}) doping," *Sci. Rep.*, vol. 5, p. 9328, 2015, doi: 10.1038/srep09328.

[18] D. Zhang *et al.*, "VO_2 thermochromic films on quartz glass substrate grown by RF plasma assisted oxide molecular beam epitaxy," *Mater*., vol. 10, p. 314, 2017, doi: 10.3390/ma10030314.

[19] L. Lu *et al.*, "Effect of Fe doping on thermochromic properties of VO_2 films," *J. Mater. Sci.: Mater. Electron.*, vol. 29, p. 5501, 2018, doi: 10.1007/s10854-018-8518-1.

[20] D. Vernardou, D. Louloudakis, E. Spanakis, N. Katsarakis and E. Koudoumas, "Thermochromic amorphous VO_2 coatings grown by APCVD using a single-precursor," *Sol. Energy Mater. Sol. Cells*, vol. 128, pp. 36, 2014, doi: 10.1016/j.solmat.2014.04.033.

[21] C. Drosos and D. Vernardou, "Advancements, challenges and prospects of chemical vapour pressure at atmospheric pressure on vanadium dioxide structures," *Mater*., vol. 11, p. 384, 2018, doi: 10.3390/ma11030384.

[22] D. A. Vinichenko, V. P. Zlomanov, V. A. Vasilev, D. S. Seregin and O. Y. Berezina, "Synthesis of vanadium dioxide films by a modified sol-gel process," *Inorg. Mater.*, vol. 47, p. 3, 2011, doi: 10.1134/S0020168511030216.

[23] G. Pan, J. Yin, K. Ji, X. Li, X. Cheng and H. Jin, "Synthesis and thermochromic property studies on W doped VO_2 films fabricated by sol-gel method," *Sci. Rep*., vol. 7, p. 6132, 2017, doi: 10.1038/s41598-017-05229-9.

[24] R. E. Marvel, K. Appavoo, B. K. Choi, J. Nag and R. F. Haglund, "Electron beam deposition of vanadium dioxide thin films," *Appl. Phys. A*, vol. 111, p. 975–981, 2013, doi: 10.1007/s00339-012-7324-5.

[25] R. E. Marvel, R. R. Harl, V. Craciun, B. R. Rogers and R. F. Haglund, "Influence of deposition process and substrate on the phase transition of vanadium dioxide thin films, *Acta Mater.*, vol. 91, p. 217, 2015, doi: 10.1016/j.actamat.2015.03.009.

[26] X. Tan *et al.*, "Unraveling metal-insulator transition mechanism of VO_2 triggered by tungsten doping," *Sci. Rep.*, vol. 2, 2012, doi: 10.1038/srep00466.

[27] S. Long *et al.*, "Effects of V_2O_3 buffer layers on sputtered VO_2 smart windows: Improved thermochromic properties, tunable width of hysteresis loops and enhanced durability," *Appl. Surf. Sci.*, vol. 441, pp. 764–772, 2018, doi: 10.1016/j.apsusc.2018.02.083.

[28] C. M. Sella, O. Nemraoui, N. Renard, & Y. Sampeur, “Preparation, characterization and properties of sputtered electrochromic and thermochromic devices,” *Surf. Coat. Technol.*, vol. 98, no. 1–3, pp. 1477–1482, 1998.

[29] M. J. Miller and J. Wang, “Multilayer ITO/VO_2/TiO_2 thin films for control of solar and thermal spectra,” *Sol. Energy Mater. Sol. Cells*, vol. 154, pp. 88–93, 2016, doi: 10.1016/j.solmat.2016.04.044.

[30] J. Zheng, S. Bao and P. Jin, “TiO_2(R)/VO_2(M)/TiO_2(A) multilayer film as smart window: Combination of energy-saving, antifogging and self-cleaning functions, *Nano Ener.*, vol. 11, pp. 136–145, 2015, doi: 10.1016/j.nanoen.2014.09.023.

[31] C. Wang, L. Zhao, Z. Liang, B. Dong, L. Wan and S. Wang, “New intelligent multifunctional SiO_2/VO_2 composite films with enhanced infrared light regulation performance, solar modulation capability, and super-hydrophobicity,” *Sci. Technol. Adv. Mater.*, vol. 18, no. 1, pp. 563–573, 2017, doi: 10.1080/14686996.2017.1360752.

[32] B. S. Khanyile, C. Mtshali, I. G. Madiba, A. Simo, N. Numan and K. Kaviyarasu, “Effect of varying the vanadium thickness layer of V_2O_5/V/V_2O_5 film on its microstructural and thermochromic properties,” *J. Vac. Sci. Technol. A*, vol. 37, no. 5, p. 051511, 2019, doi: 10.1116/1.5096249.

[33] L. Zhou, M. Xu, X. Song, P. Li, X. Qiang and J. Liang, “Modified color for VO_2/Au/VO_2 sandwich structure -based smart windows,” *Appl. Phys. A*, vol. 124, p. 505, 2018, doi: 10.1007/s00339-018-1927-4.

[34] Y.-H. Han *et al.*, “Fabrication of vanadium oxide thin film with high-temperature coefficient of resistance using V_2O_5/V/V_2O_5 multi-layers for uncooled microbolometers,” *Thin Solid Films*, vol. 425, no. 1–2, pp. 260–264, 2003, doi: 10.1016/S0040-6090(02)01263-4.

[35] Y. Zhao, R. Xu, X. Zhang, X. Hu, R. J. Knize and Y. Lu, “Simulation of smart windows in the ZnO/VO_2/ZnS sandwiched structure with improved thermochromic properties,” *Ener. Build.*, vol. 66, pp. 545–552, 2013, doi: 10.1016/j.enbuild.2013.07.071.

[36] S. Long, H. Zhou, S. Bao, Y. Xin, X. Cao and P. Jin, “Thermochromic multilayer films of WO_3/VO_2/WO_3 sandwich structure with enhanced luminous transmittance and durability,” *RSC Adv.*, vol. 108, p. 106435, 2016, doi: 10.1039/C6RA23504B.

[37] O. Sakata & M. Nakamura, “Grazing incidence X-ray diffraction,” in *Surface Science Techniques.* Springer, 2013, pp. 165–190.

[38] Y. Shvyd’ko *et al.*, “Near-100% bragg reflectivity of X-rays,” *Nat. Photon*, vol. 5, pp. 539–542, 2011, doi: 10.1038/nphoton.2011.197.

[39] N. Paul *et al.*, “Surface distortion of Fe dot-decorated TiO_2 nanotubular templates using time-of-flight grazing incidence small angle scattering,” *Sci. Rep*., vol. 10, p. 4038, 2020, doi: 10.1038/s41598-020-60899-2.

[40] A. Tselev *et al.*, Mesoscopic metal-insulator transition at ferroelastic domain walls in VO_2, *ACS Nano*., vol. 4, no. 8, pp. 4412–4419, 2010, doi: 10.1021/nn1004364.

[41] A. Tselev *et al.*, "Symmetry relationship and strain-induced transitions between insulating M1 and M2 and metallic R phases of vanadium dioxide," *Nano Lett.*, vol. 10, no. 11, pp. 4409–4416, 2010, doi: 10.1021/nl1020443.

[42] J. Wei, Z. Wang, W. Chen and D.H. Cobden, "New aspects of the metal-insulator transition in single-domain vanadium dioxide nanobeams," *Nat. Nanotechnol.*, vol. 4, no. 7, pp. 420–424, 2009, doi: 10.1038/nnano.2009.141.

[43] T. Favaloro *et al.*, "Direct observation of nanoscale peltier and joule effects at metal-insulator domain walls in vanadium dioxide nanobeams," *Nano Lett.*, vol. 14, no. 5, pp. 2394–2400, 2014, doi: 10.1021/nl500042x.

[44] E. K. H. Salje and S. Kustov, "Dynamic domain boundaries: Chemical dopants carried by moving twin walls," *Phys. Chem. Chem. Phys.*, vol. 25, no. 3, pp. 1588–1601, 2023, doi: 10.1039/D2CP04908B.

[45] K. Nagashima, T. Yanagida, H. Tanaka and T. Kawai, "Stress relaxation effect on transport properties of strained vanadium dioxide epitaxial thin films," *Phys. Rev. B*, vol. 74, p. 172106, 2006, doi: 10.1103/PhysRevB.74.172106.

[46] C. V. Ramana, R. J. Smith, O. M. Hussain and C. M. Julien, "On the growth mechanism of pulsed-laser deposited vanadium oxide thin films," *Mater. Sci. Eng. B*, vol. 111, pp. 218–225, 2004, doi: 10.1016/j.mseb.2004.04.017.

[47] L. Mathevula *et al.*, "Thermochromic VO_2 on Zinnwaldite mica by pulsed laser deposition," *Appl. Surf. Sci.*, vol. 314, pp. 476-480, 2014, doi: 10.1016/j.apsusc.2014.07.035.

[48] I-H. Hwang, C-I. Park, S. Yeo, C-J. Sun and S-W. Han, "Decoupling the metal insulator transition and crystal field effects of VO_2. *Sci. Rep.*, vol. 11, p. 3135, 2021, doi: 10.1038/s41598-021-82588-4.

[49] J. Planer, F. Mittendorfer and J. Redinger, "First principles studies of the electronic and structural properties of the rutile VO_2 (110) surface and its oxygen-rich terminations," *J. Phys. Condens.*, vol. 33, no. 47, p. 475002, 2021, doi: 10.1088/1361-648X/ac2203.

[50] E. Mohebbi, E. Pavoni, D. Mencarelli, P. Stipa, L. Pierantoni and E. Laudadio, "Insights into first-principles characterization of the monoclinic VO_2 (B) polymorph via DFT + U calculation: Electronic, magnetic and optical properties," *Nanoscale Adv.*, vol. 17, no. 4, pp. 3634–3646, 2022, doi: 10.1039/D2NA00247G.

[51] S. Zhang, J. Y. Chou and L. J. Lauhon, "Direct correlation of structural domain formation with the metal insulator transition in a VO_2 nanobeam," *Nano Lett.*, vol. 9, no. 12, p. 4527–4532, 2009, doi: 10.1021/nl9028973.

[52] E. Strelcov, A. V. Davydov, U. Lanke, C. Watts and A. Kolmakov, “In situ monitoring of the growth, intermediate phase transformations and templating of single crystal VO_2 nanowires and nanoplatelets,” *ACS Nano*, vol. 5, no. 4, pp. 3373–3384, 2011, doi: 10.1021/nn2007089.

[53] S. Zhang, I. S. Kim and L. J. Lauhon, “Stoichiometry engineering of monoclinic to rutile phase transition in suspended single crystalline vanadium dioxide nanobeams,” *Nano Lett.*, vol. 11, no. 4, pp. 1443–1447, 2011, doi: 10.1021/nl103925m.

[54] A. S. Kadari *et al.*, “Growth and characterization of transparent vanadium doped zinc oxide thin films by means of a spray pyrolysis process for TCO application,” *J. Sol-Gel Sci. Technol.*, vol. 103, pp. 691–703, 2022, doi: 10.1007/s10971-022-05875-0.